
Article:
Wang, Weiyu, Niu, Shuangxia and Zhao, Xing orcid.org/0000-0003-4000-0446 (2023) A Novel Field and Armature Synchronous Pulse Injection Method for Sensorless Drive Control of 12/10 DC Vernier Reluctance Machine. IEEE Transactions on Energy Conversion. pp. 2126-2135. ISSN: 0885-8969

https://doi.org/10.1109/TEC.2023.3268328

A Novel Field and Armature Synchronous Pulse Injection Method for Sensorless Drive Control of 12/10 DC Vernier Reluctance Machine

Weiyu Wang, Shuangxia Niu, *Senior Member, IEEE*, and Xing Zhao, *Member, IEEE*

***Abstract*- DC-excited Vernier reluctance machine (DC-VRM) exhibits the advantages of small torque ripple and high reliability, which has good potential to be applied as an aerospace starter generator. Combined with a sensorless drive, system reliability can be further guaranteed. However, the inherent self-inductance saliency is canceled out by winding connections in 12/10 DC-VRM, thus limiting the application of the self-inductance-based sensorless drive method in such machines. By revealing the saliency annihilation effect in self-inductance and the saliency enhancement effect in mutual inductance, a novel field and armature synchronous pulse injection method is proposed based on machine mutual inductance characteristics. The key is to inject detection pulses into both field and armature windings with the same sequence and pulse width to detect the mutual inductance between them. Then, an optimized virtual inductance-based position estimation method is presented to estimate the position and strengthen the fault-tolerant ability. Moreover, the potential magnetic saturation influence on position estimation caused by superimposed detection currents is avoided with the reverse pulse injection in the field winding. Consequently, the field current density can be decreased during the detection pulse injection stage. The proposed method is easy to be implemented and verified by experimental results.**

***Index Terms*—DC-excited vernier reluctance machine (DC-VRM), pulse injection, sensorless drive**

I. Introduction

From the perspective of energy-saving and environmental protection, the research of integrated starter and generator (ISG) for transportation electrification applications has attracted more attention [1-2]. As the key component of the ISG system, electrical machines are exposed to new challenges of harsh environments adaption, cost-saving and reliability [3-4]. Developing non-permanent magnet reluctance machines has been a hot research topic [5].

Switched reluctance machine (SRM) suffers from severe torque ripple and noises [6]. Doubly-fed doubly salient machine (DF-DSM) has unbalanced magnetic distribution and rich even-order flux harmonics [7]. Compared with these counterparts, more flexible slot pole combinations can be applied in DC-excited vernier reluctance machine (DC-VRM), which has small torque ripple and the minimum cogging torque [8-9]. Therefore, DC-VRM can be esteemed as a potential rare-earth-free cost-efficient solution to be applied as ISG.

Combined with a position-sensorless drive, system cost can be further decreased, and system reliability can be guaranteed accordingly [10]. For doubly salient reluctance machines, the research of high-speed sensorless drive based on back-EMF or flux linkage has been relatively mature, but their low signal-to-noise ratio constrains their application in zero and low-speed ranges [11]. For low-speed sensorless drive, modulation method [12], sense coil method [13], current waveform method [14-16], and pulse injection method [17-26] are typical strategies. In the modulation method, a carrier signal is generated by an oscillator, and the idle phase inductance information is modulated [12-13]. A demodulation circuit is required to calculate position, and a switching circuit is required to separate the detection circuit and the drive circuit. Without the switching circuit, sense coil method usually embeds a small number of turns of the sense coil inside the motor, so that the detection coil is separated from the armature windings [13]. In this way, the motor drive system is relatively independent of the position detection system. However, this method is not easy to assemble and requires additional detection circuits. Current waveform method does not require additional hardware, it detects the current slop and combines the incremental inductance model to estimate rotor position [14-16]. Unfortunately, this method cannot be applied to estimate the rotor initial position.

In pulse injection methods, by injecting narrow detection pulses into idle phases, inductance can be detected indirectly. As the detection pulse width is very small, the saturation effect can be ignored. In addition, this method can perform well in both zero and low-speed ranges. However, due to the half-cycle conduction principle of SRM, negative torque is generated, and full-cycle inductance detection cannot be achieved. To decrease the influence of negative torque generation, the induced current reduction method is developed [17-18]. To acquire the full-cycle inductance, the pulse injection method is combined with the current waveform method to obtain the full-cycle inductance [19]. For DF-DSM, full-cycle inductance can be acquired by the pulse injection method only [20]. In addition, the negative torque generation can be avoided by adjusting the directions of detection pulses [21].

For the magnetic characteristics-based position estimation method, the premeasurement procedure is time-consuming, and the 3-D lockup table occupies large memory storage [22]. To save microprocessor storage memory, the inductance threshold

This work was supported by the National Natural Science Foundation of China under Project 52077187 and in part by the Research Grant Council of the Hong Kong Government under Project PolyU 152143/18E and PolyU 152109/20E. (*Corresponding author: Shuangxia Niu.*)

Weiyu Wang and Shuangxia Niu are with the Department of Electrical Engineering, The Hong Kong Polytechnic University, Hong Kong. (e-mail: weiyu.wang@connect.polyu.hk; eesxniu@polyu.edu.hk)

Xing Zhao is with the Department of Electronic Engineering, University of York, United Kingdom. (e-mail: xing.zhao@york.ac.uk;)

method [24] can detect the switching point but cannot acquire an accurate rotor position. For SRM, the inductance model can be simplified by considering DC and first-order harmonics only [26]. However, as other inductance harmonics are ignored, position estimation accuracy cannot be guaranteed. A second-order inductance harmonic is introduced for position estimation in the selected inductance region [27]. Compared with the above magnetic characteristics-based method, the inductance modeling methods without complex measurements and large memory storage are more attractive. The inductance vector method is proposed in [28] for rotor initial position estimation and expanded for the start-up stage in [19]. The inductance modeling process is simplified by assuming the inductance as a sinusoidal wave. Due to the existence of inductance model mismatch, complex coordination transformation [29] or online calibration [30] is required to cancel the DC or third-order harmonics influence.

For the 12/10 DC-VRM, a saliency annihilation phenomenon occurs in self-inductance, thus constraining the application of the self-inductance-based sensorless drive method [25,33]. By analyzing the harmonics distributions of self-inductance and mutual inductance through Fourier analysis, the saliency annihilation effect in self-inductance and the saliency enhancement effect in mutual inductance are revealed. It means that the position-sensorless drive for the studied DC-VRM can be designed based on mutual inductance saliency. In previous studies, the mutual inductance voltage method in SRM is constrained by a low signal-to-noise ratio and its dependence on additional detection circuits [31]. For DF-DSM, the mutual inductance voltage method is only applied for initial position estimation, and the system cost and weight are increased by additional terminal voltage sensors [32].

In this paper, a novel field and armature synchronous pulse injection method (FA-SPIM) is proposed based on the machine mutual inductance model. The advantages of pulse injection methods are kept, and no additional detection equipment is required. In addition, system cost can be decreased compared with existing dual-inverter and H-bridge converter drive topologies for DC-VRM. The key is to inject detection pulses into the field and the armature windings with the same sequence and pulse width to detect the mutual inductances. Reliable position estimation can be achieved by combining the inductance vector modeling method, and then an optimized virtual inductance vector-based position estimation method is presented to strengthen fault-tolerant ability. Moreover, to avoid the potential magnetic saturation influence caused by the superimposed detection currents, the proposed method is optimized as field winding reverse pulse injection. The proposed FA-SPIM can be applied to a group of non-salient DC-VRM. The arrangements of this paper are as follows. In Section II, the configuration and the mathematical model of DC-VRM are introduced. In Section III, the inductance characteristics of DC-VRM are analyzed. In Section IV, the FA-SPIM is proposed and optimized as field winding reverse pulse injection and virtual inductance-based position estimation. In Section V, experimental results are presented. Finally, some conclusions are drawn.

II. Principle of 12/10 DC-VRM

A. Configuration of 12/10 DC-VRM

As illustrated in Fig .1, ISG can work as a starter to start up the machine and operates as a generator for energy recycling. Through this integrated design, system volume, weight and costs can be decreased. The machine structure and the drive topology of the 12/10 DC-VRM are provided in Fig. 2(a) and Fig. 2(b), respectively. The DC field coils are wound on each stator tooth, and the directions of the two adjacent DC field coils are opposite. The AC armature coils are wound on each stator tooth as well. Two sets of armature coils that have 180° phase differences are reversely cascaded to form one single phase.

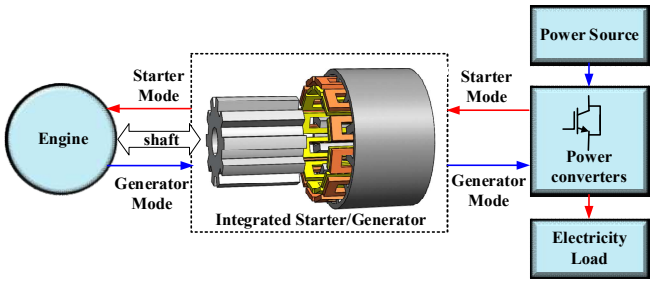

Fig. 1. Integrated starter and generator system.

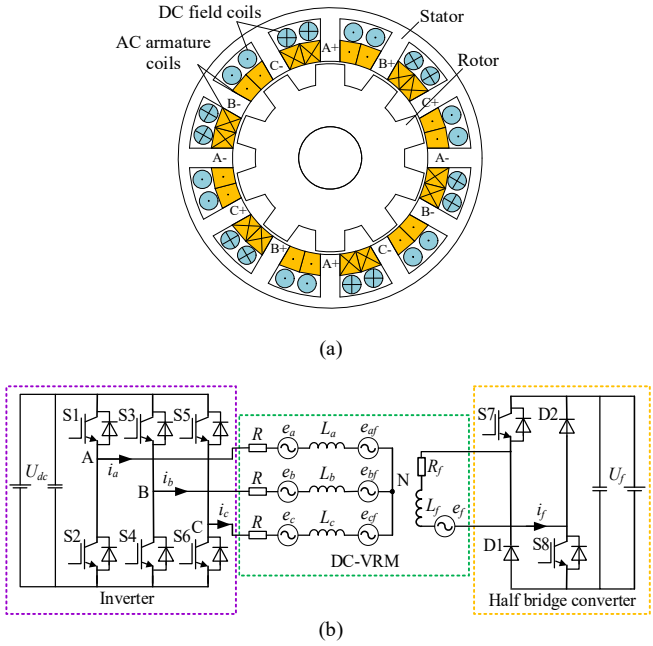

Fig. 2. The driving system for 12/10 DC-VRM. (a) Structure of 12/10 DC-VRM. (b) Drive topology of 12/10 DC-VRM.

B. Mathematical Model of DC-VRM

The current, inductance and torque equations of DC-VRM can be expressed as

$$I=[i_a \quad i_b \quad i_c \quad i_f]^T \tag{1}$$

$$L=\begin{bmatrix} L_a & M_{ab} & M_{ac} & M_{af} \\ M_{ab} & L_b & M_{bc} & M_{bf} \\ M_{ac} & M_{bc} & L_c & M_{cf} \\ M_{af} & M_{bf} & M_{cf} & L_f \end{bmatrix} \quad (2)$$

$$T=\frac{1}{2}I^T\frac{dL}{d\theta}I \quad (3)$$

where I is the current matrix, i_a, i_b and i_c are armature currents, i_f is the field current, L is the inductance matrix, M_{af}, M_{bf} and M_{cf}, are the mutual inductances between the field winding and the armature windings, L_a, L_b and L_c are the phase self-inductances, M_{ab}, M_{ac} and M_{bc} are the mutual inductances between armature windings, L_f is the self-inductance of the field winding, T is the total torque, θ is the electrical angle. The torque generated by phase A can be expanded as

$$T_a=i_a i_f\frac{dL_{af}}{d\theta}+\frac{1}{2}i_a^2\frac{dL_a}{d\theta}+\frac{1}{2}i_f^2\frac{dL_f}{d\theta} \quad (4)$$

The first term is the excitation torque produced by the mutual inductance between the field winding and the armature winding. The second and the third term are the reluctance torque and the cogging torque, respectively.

III. Fourier Analysis of Inductance Characteristics

A. Self-inductance Characteristics

To further analyze the inductance characteristics, Fourier analysis is introduced [25,33]. For example, phase A is composed of coils A+ and A-. As coils A+ and A- have 180° phase differences, the Fourier expansion of their self-inductance L_{a+} and L_{a-} can be expressed as

$$L_{a+}=L_{adc}+\sum L_n\sin(n\omega t+\theta_n) \quad , \quad n=1,2,3\ldots. \quad (5)$$

$$L_{a-}=L_{adc}+\sum L_n\sin(n\omega t+n\pi+\theta_n) \quad , \quad n=1,2,3\ldots. \quad (6)$$

where L_{adc} is the DC component of self-inductance. L_n is the amplitude of the nth harmonics, ω is the electrical angular velocity, θ_n is the initial phase angle of the nth harmonics. The Fourier expansion of the self-inductance of phase A L_a can be regarded as the composition of coils A+ and A-.

$$L_a=L_{a+}+L_{a-}=2L_{adc}+2\sum L_n\sin(n\omega t+\theta_n) \quad , \quad n=2,4,6\ldots. \quad (7)$$

As shown in Eq. (7), the DC component is doubled while a saliency annihilation phenomenon occurs in L_a. The odd-order harmonics including the fundamental component are canceled when they are superimposed. As a doubly salient machine, the saliency effect mainly exists in the fundamental harmonic component. This phenomenon constrains the application of self-inductance saliency tracking sensorless drive methods.

B. Mutual Inductance Characteristics

M_{af+} and M_{af-} are the mutual inductance between field coils and the armature coils A+ and A-, respectively. Their Fourier expansion can be illustrated as

$$M_{af+}=M_{afdc}+\sum M_n\sin(n\omega t+\alpha_n) \quad , \quad n=1,2,3\ldots. \quad (8)$$

$$M_{af-}=M_{afdc}+\sum M_n\sin(n\omega t+n\pi+\alpha_n) \quad , \quad n=1,2,3\ldots. \quad (9)$$

where L_{afdc} is the DC component of mutual inductance. M_n is the amplitude of the nth harmonics, ω is the electrical angular velocity, α_n is the initial phase angle of the nth harmonics. As coils A+ and A- have a 180° phase difference, the Fourier expansion of the mutual inductance between phase A and the field coils is

$$M_{af}=M_{af+}-M_{af-}=2\sum M_n\sin(n\omega t+\theta_n) \quad , \quad n=1,3,5\ldots. \quad (10)$$

It is clear to see from the final mutual inductance equation that the DC component and all the even-order harmonics are canceled, and all the odd-order harmonics including the fundamental component are doubled. Therefore, the saliency enhancement effect in mutual inductance is revealed, and this characteristic can be applied to position estimation.

The self-inductance, mutual inductance and their harmonics distributions acquired by finite element analysis (FEA) are presented in Fig. 3. Through this analysis, a self-inductance annihilation phenomenon in DC-VRM is revealed, and the mutual inductance saliency characteristics have been strengthened. Therefore, the design for a 12/10 DC-VRM position-sensorless drive should be mutual inductance dependent, rather than self-inductance dependent.

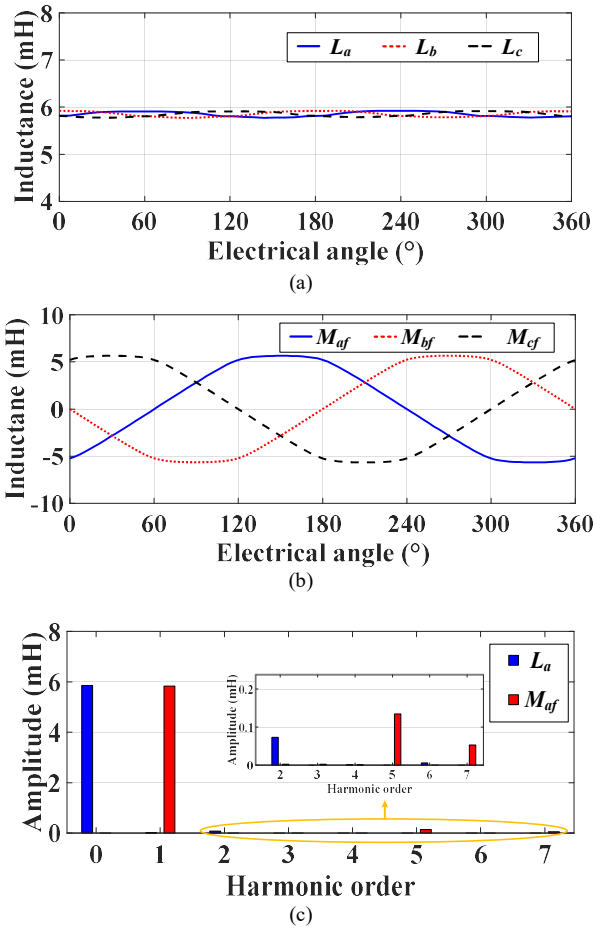

Fig. 3. FEA results. (a) Self-inductances. (b) Mutual inductances. (c) Harmonics distributions.

IV. Field and Armature Windings Synchronous Pulse Injection Sensorless Drive

A. Traditional Pulse Injection Self-inductance Detection Method

The pulse injection method is an indirect inductance detection method [19]. As shown in Fig .4, when a detection pulse is injected into the armature winding, the equivalent voltage of the series armature winding can be expressed as

$$U_{dc}=L_{a+c}\frac{di_a}{dt}+e_{a+c}+2i_aR \tag{11}$$

where U_{dc} is the DC voltage supply, L_{a+c} is the series self-inductance of armature winding, i_a is the resultant current of detection pulse, e_{a+c} is the back-EMF of the series winding, and R is the resistance of the armature winding. In the low-speed range, e_{a+c} can be overlooked. In addition, as the detection pulse width is small, thereby the resultant current is small. The winding voltage drop can be ignored. L_{a+c} can be expressed as

$$L_{a+c}=\frac{U_{dc}\Delta t}{\Delta i_a} \tag{12}$$

where Δt is the detection pulse width, and Δi_a is the increment of the resultant current of phase A.

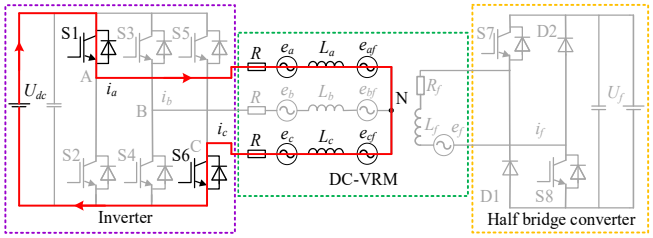

Fig. 4. Equivalent circuit of armature winding detection pulse injection.

Through the detection pulse method, the self-inductance of the series armature winding can be estimated. However, a saliency annihilation phenomenon occurs in self-inductance of 12/10 DC-VRM, the self-inductances only show small fluctuations in the whole electrical period. Therefore, it is difficult to distinguish the inductance amplitudes through the detection pulses.

B. Proposed Field and Armature Synchronous Pulse Injection Sensorless Drive Method

To detect the mutual inductance between the field winding and armature windings, a novel FA-SPIM is proposed based on machine mutual inductance saliency. As illustrated in Fig .5, the key is to inject detection pulses with the same pulse width into the field winding and the series armature winding simultaneously. Then the mutual inductance can be solved through the voltage equations. During the pulse injection stage, the voltage equations of the field winding and the series armature winding can be expressed as Eq. (13) and Eq. (14), respectively.

$$U_{dc}=L_{a+c}\frac{di_a}{dt}+(M_{af}-M_{cf})\frac{di_f}{dt} \tag{13}$$

$$U_f=L_f\frac{di_f}{dt}+(M_{af}-M_{cf})\frac{di_a}{dt} \tag{14}$$

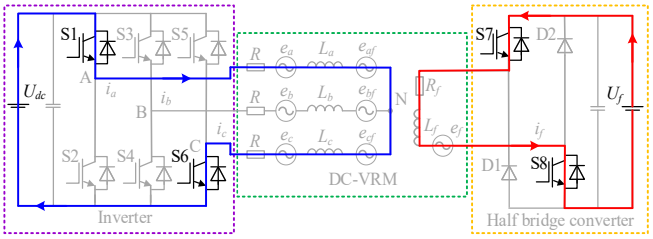

Fig. 5. Equivalent circuit of FA-SPIM.

where U_f is the DC voltage supply of the half-bridge converter. During this stage, the power transistor states will not change, and the voltage equations of the field winding and the series armature winding are kept. Therefore, the series mutual inductance M_{acf} can be solved as

$$M_{acf}=M_{af}-M_{cf}=\frac{U_f-L_{a+c}\frac{\Delta i_a}{\Delta t}}{\frac{\Delta i_f}{\Delta t}}=\frac{U_f\Delta t-\Delta i_aL_{a+c}}{\Delta i_f} \tag{15}$$

where Δi_f is the increment of the resultant current of the field winding. Similarly, by operating power transistors stages, the remained mutual inductances M_{baf} and M_{cbf} between the remained armature windings and the field windings can be detected. To be more specific, the principle of the proposed method is illustrated in Fig .6. From t_1 to t_2, the detection pulses are only injected into the armature windings to detect the self-inductances. From t_2 to t_3, field and armature synchronous pulses are injected, and their injection sequence and pulse width are kept the same. As the mutual inductance coupling is introduced, the resultant currents become different from the self-inductance detection stage. By calculating the rotor position, the conduction phases are determined, and the field winding is excited during t_3 and t_4. Acceleration pulses are defined as gate signals to drive the machine during the current chopping control stage. These pulses injected from t_4 to t_5 are decided by the estimated position and the current chopping regulator. A new round of detection pulses is injected from t_6.

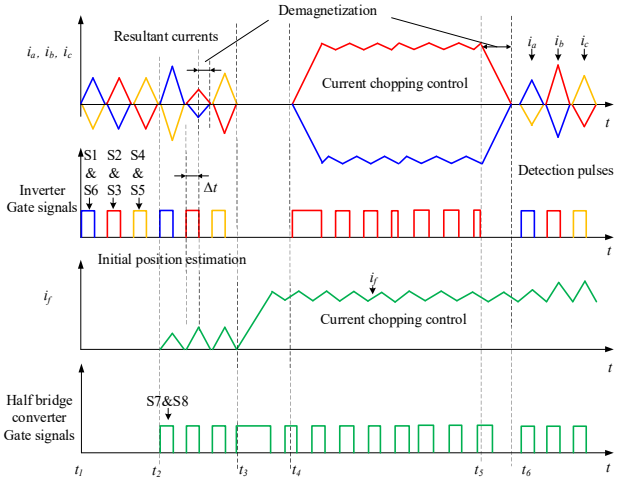

Fig. 6. Schematic diagram of FA-SPIM.

C. Virtual Inductance Vector based Position Estimation

The inductance vector-based position estimation method [19,28] is an effective strategy to estimate rotor position without prior knowledge but requires an assumption of ideal sinusoidal inductance. In previous research, complex coordination transformation [29] or online calibration [30] are required to cancel the DC, third or even-order harmonics. In existing methods, the inductance Fourier model with maximum secondary inductance harmonic can offer good estimation accuracy [11]. As revealed in Fig .3, the DC, third and all the even-order mutual inductance harmonics are canceled out in the studied DC-VRM due to its complementary structure, which means, even an inductance Fourier model with a maximum 4th harmonic can be represented as an ideal sinusoidal model. In addition, the amplitudes of the 5th and 7th inductance harmonics are very small. So, the series mutual inductance model can be established as the ideal sinusoidal model in Fig. 7. For this reason, the inductance vector-based position estimation method is quite suitable for the studied machine. An optimized virtual inductance vector-based position estimation method is presented to strengthen fault-tolerant ability. Taking M_{acf} as an example, when current sampling failure occurs in this phase, mutual inductance value cannot be detected directly. As the sum of three series mutual inductance is zero, a virtual inductance M'_{acf} can be described by Eq. (16).

$$M'_{acf}=-M_{baf}-M_{cbf} \tag{16}$$

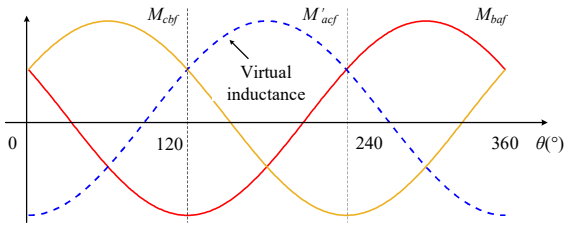

Fig. 7. Series mutual inductances of 12/10 DC-VRM.

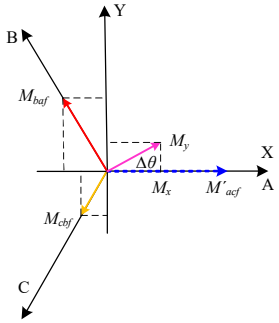

Fig. 8. Virtual inductance vector orthogonal decomposition.

As shown in Fig .8, the rotor position of the composing series mutual inductance vector $\Delta\theta$ can be decomposed through orthogonal decomposition [19,28] by the following equations.

$$M_x=M'_{acf}-\frac{1}{2}(M_{baf}+M_{cbf}) \tag{17}$$

$$M_y=\frac{\sqrt{3}}{2}(M_{baf}-M_{cbf}) \tag{18}$$

$$\Delta\theta=arctan(\frac{M_y}{M_x}) \tag{19}$$

By comparing the amplitudes of the series mutual inductances, the rotor position sector can be determined by Table I. Then rotor position in different sectors can be solved by the following equation. Through the presented virtual inductance vector-based position estimation method, the actual inductance vector can be described by virtual inductance vector, thereby certain fault-tolerant ability can be provided when the system is exposed to inductance sampling failure.

$$\theta=\begin{cases}60\text{-}arctan[\dfrac{\frac{\sqrt{3}}{2}(M_{baf}-M_{cbf})}{M'_{acf}-\frac{1}{2}(M_{baf}+M_{cbf})}] & \text{sector=1,2}\\ 180\text{-}arctan[\dfrac{\frac{\sqrt{3}}{2}(M_{baf}-M_{cbf})}{M'_{acf}-\frac{1}{2}(M_{baf}+M_{cbf})}] & \text{sector=3,4}\\ 300\text{-}arctan[\dfrac{\frac{\sqrt{3}}{2}(M_{baf}-M_{cbf})}{M'_{acf}-\frac{1}{2}(M_{baf}+M_{cbf})}] & \text{sector=5,6}\end{cases} \tag{20}$$

TABLE I
RELATION BETWEEN ELECTRICAL ANGLE, MUTUAL INDUCTANCES, CONDUCTION PHASES AND ROTOR SECTOR

θ (°)	Inductance relation	Conduction phases	Sector
0-60	$M_{cbf}>M_{baf}>M'_{acf}$	A and B	I
60-120	$M_{cbf}>M'_{acf}>M_{baf}$	A and C	II
120-180	$M'_{acf}>M_{cbf}>M_{baf}$	B and C	III
180-240	$M'_{acf}>M_{baf}>M_{cbf}$	B and A	IV
240-300	$M_{baf}>M'_{acf}>M_{cbf}$	C and A	V
300-360	$M_{baf}>M_{cbf}>M'_{acf}$	C and B	VI

D. Optimized Field Winding Reverse Pulses Injection Method Considering magnetic saturation

During the initial position estimation stage, the magnetic saturation effect does not need to be considered in the pulse injection sensorless drive method for the doubly salient machine. That is because the detection pulse width is very small, and the resultant current is limited. However, as the schematic diagram of the acceleration stage, which is shown in Fig .9, the field winding is still in an energized state, and the detection pulses are injected simultaneously. Consequently, the superimposed resultant currents of the detection pulses may increase the field current density, thus increasing the potential magnetic saturation risk. As a result, the reliability of position estimation cannot be guaranteed.

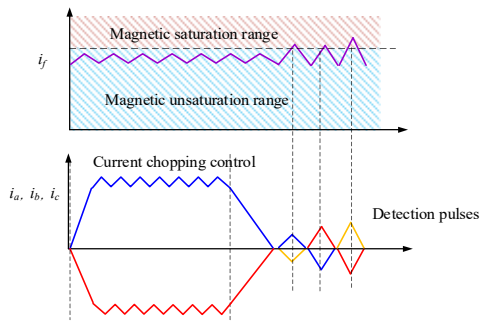

Fig .9 Schematic diagram of FA-SPIM in the acceleration stage.

To ease the influence of the superimposed resultant currents of detection pulses in the field winding, the proposed FA-SPIM is optimized with field winding reverse pulse injection. As shown in Fig. 10, when a detection pulse is injected into the armature winding, power transistors S7 and S8 are switched off to make the field winding demagnetization.

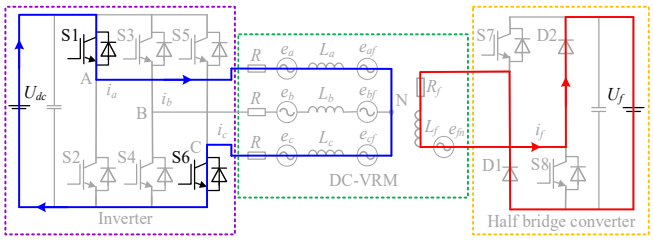

Fig. 10. Equivalent circuit of FA-SPIM optimized by the field winding reverse pulses injection.

To be more specific, the schematic diagram of the optimized FA-SPIM with field winding reverse pulse injection is illustrated in Fig .11. The detection pulses are reversely injected into the field winding. In this way, the field current density is constrained, thus guaranteeing that mutual inductances are detected in the magnetic unsaturation range. Therefore, the position estimation reliability can be guaranteed.

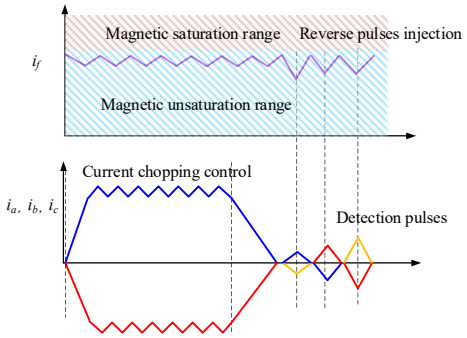

Fig. 11. Schematic diagram of FA-SPIM optimized by the field winding reverse pulse injection.

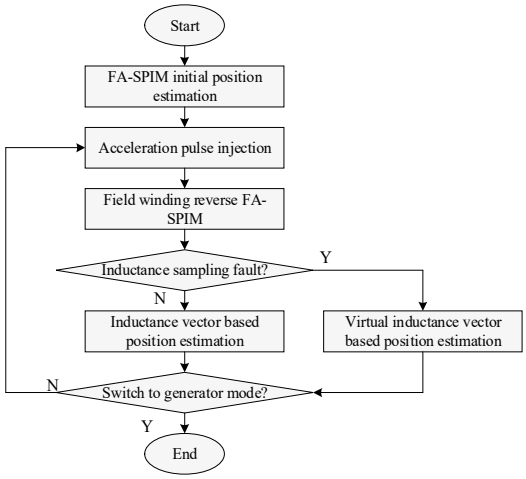

Fig. 12. Flowchart of the sensorless drive as ISG based on FA-SPIM.

E. Sensorless Drive as ISG

Fig. 12 shows the implementation of FA-SPIM for 12/10 DC-VRM. First, FA-SPIM is applied to detect the initial position, and the acceleration pulses are injected to start up the machine. During the acceleration stage, the optimized FA-SPIM with field winding reverse pulse injection method is adopted. In this way, the speed of the machine can increase steadily. When an inductance sampling fault occurs, a virtual inductance vector is calculated for position estimation. When the machine reaches the idle speed, the system can be switched to generator mode.

V. Experimental Results

A. Experimental Setup

As shown in Fig.13, to verify the proposed FA-SPIM, experiments are performed based on dSPACE MicroLabBox. The variables and parameters can be monitored through ControlDesk. An inverter and half-bridge converter are applied to drive the DC-VRM. A coaxial magnetic powder brake is connected to the DC-VRM. An oscilloscope is applied to sample the data.

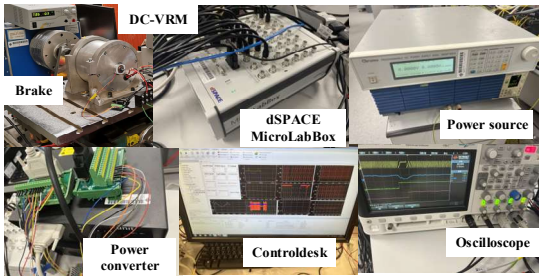

Fig. 13. Experimental setup of the proposed DC-VRM sensorless drive.

B. FA-SPIM Initial Position Estimation based on Mutual Inductance Model

The experimental result of initial position estimation is shown in Fig .14. First, the detection pulses are only injected into the armature windings to detect the self-inductances. Then, field and armature synchronous pulses are injected to detect the series mutual inductances. Through the established series mutual inductance model, initial position estimation can be acquired.

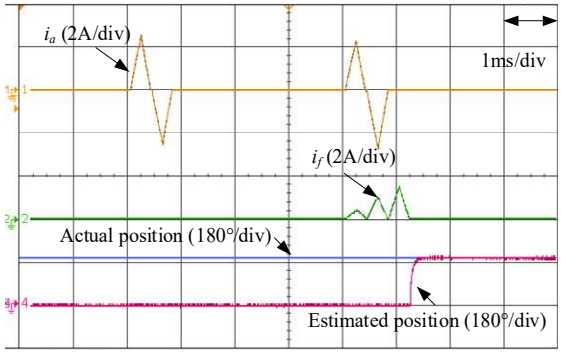

Fig. 14. FA-SPIM for initial position estimation.

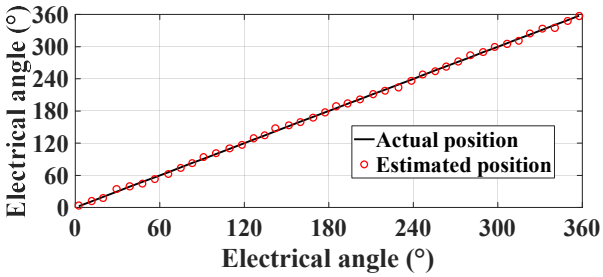

(a)

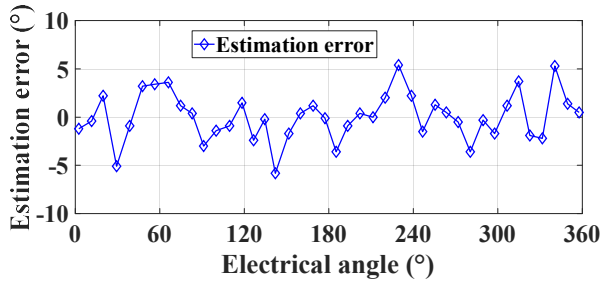

(b)

Fig. 15. FA-SPIM initial position estimation. (a) Position estimation in an electrical angle period. (b) Estimation error.

To further verify the established mutual inductance model for position estimation, the rotor is manually placed at different initial positions and the proposed FA-SPIM is applied to detect the mutual inductances and then identify the initial position in the whole electrical angle period. The actual position and the estimated position are compared in Fig .15(a). As shown in Fig .15(b), the estimation error can be controlled with the range of 6° electrical angle, corresponding to 0.6° of rotor angle in the whole electrical period. To evaluate the proposed method further quantitatively, the root means square error (RMSE) is introduced and defined by the following equation.

$$\mathrm{RMSE}=\sqrt{\frac{1}{n}\sum_{j=1}^{n} e_j} \tag{21}$$

where n is the number of the sampled points in Fig. 15(a), j is the number of the sampling, and e_j is the error of the *j-th* sampling. In this experiment, RMSE is 2.34° electrical angle, corresponding to 0.234° mechanical angle.

C. FA-SPIM Optimized by Field Winding Reverse Pulses Injection and Virtual Inductance Vector-based Sensorless Operation

The proposed FA-SPIM optimized by field winding reverse pulse injection is testified by experiments. The detection pulse width and acceleration pulse width are designed as 0.2ms and 1.7ms, respectively. The load torque is 2Nm. It is clear to see in Fig .16 that the proposed method can effectively detect the series mutual inductances. The three series mutual inductances M_{acf}, M_{baf} and M_{cbf} are symmetrical and combined with the established series mutual inductances model, position estimation can be achieved.

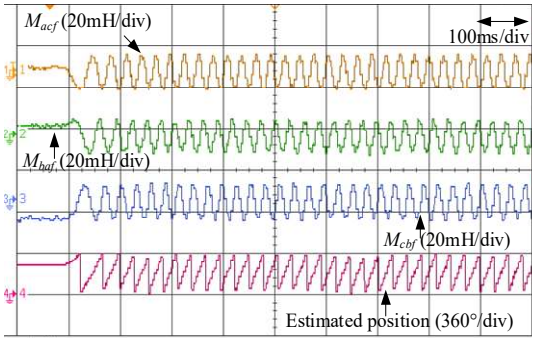

Fig. 16. Estimated mutual inductances and position.

As shown in Fig. 17, to verify the effectiveness of the presented virtual inductance vector-based position estimation method, FA-SPIM is operated with virtual inductance vector-based position estimation to start up the machine. The proposed method can effectively start up the machine, and the rotor speed can reach 250rpm smoothly. Field winding reverse pulses injection. Through this method, the current level of the field winding can be decreased, and thereby the potential magnetic saturation risk can be avoided.

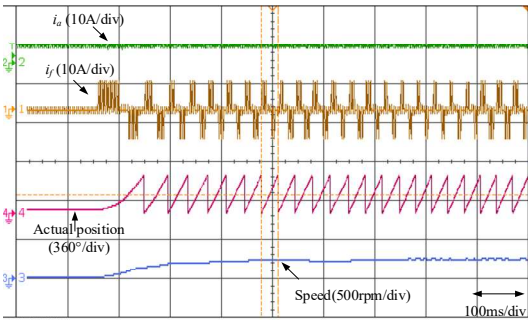

(a)

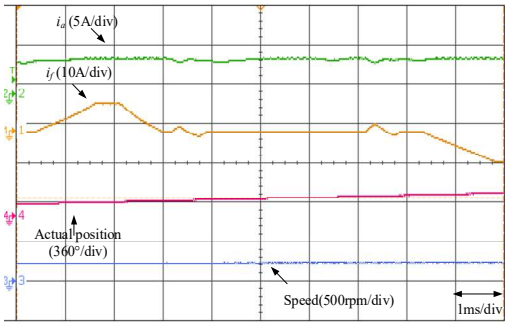

(b)

Fig. 17. FA-SPIM sensorless startup. (a) Current response during the startup stage. (b) Zoomed in view.

The experimental result of transmission from actual inductance vector-based sensorless operation to virtual inductance vector-based sensorless operation is presented in Fig. 18. The measured inductance M_{acf} is forced to zero to simulate

the fault condition, and then after 0.2s delay, the system is switched to virtual inductance vector based sensorless operation. A smooth transmission between two operation modes can be found, thereby fault-tolerant ability can be provided when an inductance sampling fault occurs.

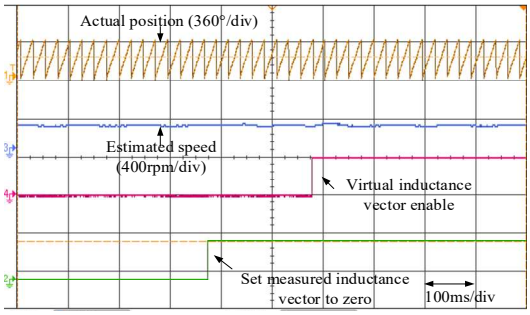

Fig. 18. Transmission from actual inductance-based sensorless operation to virtual inductance vector-based sensorless operation.

As shown in Fig. 19, during the low-speed operation range, the estimated position is compared with the actual position, and the position estimation error can be controlled with a small vibration range. Therefore, the reliability of the system can be guaranteed. The specific parameters for the studied DC-VRM are listed in Table II.

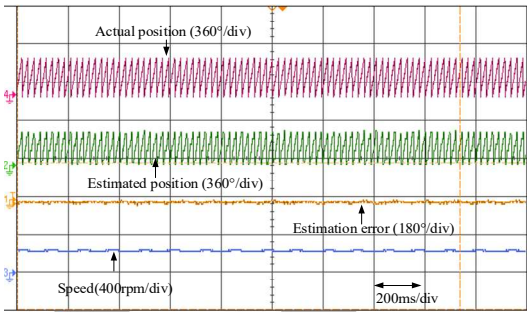

Fig. 19. Position estimation during FA-SPIM sensorless drive.

TABLE II
SPECIFIC PARAMETERS FOR THE DC-VRM

Symbol	Parameter	Unit	Value
d_{so}	Outer diameter of stator	mm	130
d_{si}	Inner diameter of stator	mm	90
d_{ro}	Outer diameter of rotor	mm	89
d_{ri}	Inner diameter of rotor	mm	60
α_s	Stator pole arc	°	12
α_r	Rotor pole arc	°	18
δ	Air gap length	mm	0.5
l	Stack length	mm	80
N_{dc}	Turns of each DC coil	-	48
N_{ac}	Turns of each AC coil	-	48
R	Sub-phase winding resistance	Ω	0.7
R_f	Field winding resistance	Ω	4.2
	Rated torque	Nm	2.4
	Rated speed	r/min	450

DISCUSSION

In this research, a novel field and armature winding synchronous pulse injection method is proposed to deal with the position sensorless drive of 12/10 DC-VRM. The feasibility and effectiveness of the proposed method are verified. It should be noticed that the proposed method belongs to the pulse injection sensorless drive method, so it is exposed to the inherent problems caused by pulse injection such as torque production and switching losses. In this study, the pulse width of the reverse injection pulse is relatively small, thus producing a very slight influence on the field current level and associated torque production. In addition, the injected pulses can be seen as a short-period switching mode that is inserted into the inherent current chopping mode. The switching loss is not a severe problem, and this loss becomes acceptable by considering the benefits that bring by reliable position sensorless operation. To mitigate the pulse injection influence on torque production and switching loss, optimization methods such as lowered pulse injection method and reduced pulse injection methods can be combined in future research [17,18,34].

CONCLUSION

This paper presents a novel field and armature synchronous pulse injection method for sensorless drive control of non-salient 12/10 DC-VRM. First, the saliency annihilation phenomenon in self-inductance and the saliency enhancement in mutual inductance are revealed through Fourier analysis, and a novel FA-SPIM is proposed. The key is to inject detection pulses into both field winding and the armature windings with the same sequence and pulse width, thereby reliable mutual inductance detection can be achieved for position estimation of non-salient DC-VRM. As the DC, third and all the even-order inductance harmonics are canceled out by machine complementary structure, the inductance vector-based position estimation method is introduced for position estimation, and then optimized with virtual inductance vector-based position estimation method to strength fault-tolerant ability. To avoid the potential magnetic saturation caused by superimposed detection currents, the proposed FA-SPIM is optimized with field winding reverse pulse injection. Through the proposed method, reliable sensorless operation can be achieved. The initial position estimation error can be controlled within the range of 0.6° rotor angle. The proposed method is easy to be implemented and does not require additional detection circuits.

ACKNOWLEDGMENT

This work was supported by the National Natural Science Foundation of China under Project 52077187 and in part by the Research Grant Council of the Hong Kong Government under Project PolyU 152143/18E and PolyU 152109/20E.

REFERENCES

[1] B. Sarlioglu and C. T. Morris, "More Electric Aircraft: Review, Challenges, and Opportunities for Commercial Transport Aircraft," *IEEE Trans. Transp. Electrif.*, vol. 1, no. 1, pp. 54-64, June 2015.

[2] V. Madonna, P. Giangrande and M. Galea, "Electrical Power Generation in Aircraft: Review, Challenges, and Opportunities," *IEEE Trans. Transp. Electrif.*, vol. 4, no. 3, pp. 646-659, Sept. 2018.

[3] R. Bojoi, A. Cavagnino, A. Tenconi and S. Asheton, "Control of Shaft-Line-Embedded Multiphase Starter/Generator for Aero-Engine," *IEEE Trans. Ind. Electron.*, vol. 63, no. 1, pp. 641-652, Jan. 2016.

[4] M. Cheng, W. Hua, J. Zhang and W. Zhao, "Overview of Stator-Permanent Magnet Brushless Machines," *IEEE Trans. Ind. Electron.*, vol. 58, no. 11, pp. 5087-5101, Nov. 2011.

[5] I. Boldea, L. N. Tutelea, and D. Dorrell, "Automotive electric propulsion systems with reduced or no permanent magnets: an overview," *IEEE Trans. Ind. Electron.*, vol. 61, no. 10, pp. 5696-5711, Oct. 2014.

[6] Y. Jin, B. Bilgin, and A. Emadi, "An extended-speed low-ripple torque control of switched reluctance motor drives," *IEEE Trans. Power Electronics*, vol. 30, pp. 1457-1470, 2015.

[7] Y. Wang, S. Niu and W. Fu, "Electrical-Continuously Variable Transmission System Based on Doubly Fed Flux-Bidirectional Modulation," *IEEE Trans Ind. Electron.*, vol. 64, no. 4, pp. 2722-2731, April 2017.

[8] X. Liu and Z. Q. Zhu, "Stator rotor pole combinations and winding configurations of variable flux reluctance machines," *IEEE Trans. Ind. Appl.*, vol. 50, no. 6, pp. 3675-3684, Nov.-Dec. 2014.

[9] S. Jia, R. Qu, J. Li, D. Li and H. Lu, "Design considerations of stator DC-winding excited vernier reluctance machines based on the magnetic gear effect," *IEEE Trans. Ind. Appl.*, vol. 53, no. 2, pp. 1028-1037, March-April 2017.

[10] G. Wang, M. Valla and J. Solsona, "Position Sensorless Permanent Magnet Synchronous Machine Drives—A Review," *IEEE Trans Ind. Electron.*, vol. 67, no. 7, pp. 5830-5842, July 2020.

[11] D. Xiao, S. R. Filho, G. Fang, J. Ye and A. Emadi, "Position-Sensorless Control of Switched Reluctance Motor Drives: A Review," *IEEE Trans. Transp. Electrif.*, vol. 8, no. 1, pp. 1209-1227, March 2022.

[12] M. Ehsani, I. Husain and A. B. Kulkarni, "Elimination of discrete position sensor and current sensor in switched reluctance motor drives," *IEEE Trans. Ind. Appl.*, vol. 28, no. 1, pp. 128-135, Jan.-Feb. 1992.

[13] Rafael, S., P. J. Costa Branco, and A. J. Pires. "Srm Sensorless for Position Control Based on a Frequency Modulation System." *Measurement: Journal of the International Measurement Confederation* 146 (2019): 171-78.

[14] J. Ye, B. Bilgin and A. Emadi, "Elimination of Mutual Flux Effect on Rotor Position Estimation of Switched Reluctance Motor Drives," *IEEE Trans. Power Electron.*, vol. 30, no. 3, pp. 1499-1512, March 2015.

[15] J. Cai and Z. Liu, "An Unsaturated Inductance Reconstruction Based Universal Sensorless Starting Control Scheme for SRM Drives," *IEEE Trans. Ind. Electron.*, vol. 67, no. 11, pp. 9083-9092, Nov. 2020.

[16] L. Ge, J. Zhong, C. Bao, S. Song and R. W. De Doncker, "Continuous Rotor Position Estimation for SRM Based on Transformed Unsaturated Inductance Characteristic," *IEEE Trans. Power Electron.*, vol. 37, no. 1, pp. 37-41, Jan. 2022.

[17] J. Cai, Y. Yan, W. Zhang and X. Zhao, "A Reliable Sensorless Starting Scheme for SRM With Lowered Pulse Injection Current Influences," *IEEE Trans. Instrum. Meas.*, vol. 70, pp. 1-9, 2021, Art no. 1003209.

[18] D. Xiao *et al.*, "Induced Current Reduction in Position-Sensorless SRM Drives Using Pulse Injection," *IEEE Trans. Ind. Electron.*, 2022, doi: 10.1109/TIE.2022.3183275.

[19] J. Cai and Z. Deng, "Sensorless control of switched reluctance motor based on phase inductance vectors," *IEEE Trans. Power Electron.*, vol. 27, no. 7, pp. 3410–3423, 2012.

[20] X. Zhou, B. Zhou and K. Wang, "Position Sensorless Control for Doubly Salient Electromagnetic Machine with Improved Startup Performance," *IEEE Trans. Ind. Electron.*, vol. 67, no. 3, pp. 1782-1791, March 2020.

[21] X. Zhou, B. Zhou and J. Wei, "A Novel Position-Sensorless Startup Method for DSEM," *IEEE Trans. Ind. Appl.*, vol. 54, no. 6, pp. 6101-6109, Nov.-Dec. 2018.

[22] J. Bu and L. Xu, "Eliminating starting hesitation for reliable sensorless control of switched reluctance motors," *IEEE Trans. Ind. Appl.*, vol. 37, no. 1, pp. 59-66, Jan.-Feb. 2001.

[23] W. Wang, X. Zhao, S. Niu and W. Fu, "Comparative Analysis and Optimization of Novel Pulse Injection Sensorless Drive Methods for Fault-Tolerant DC Vernier Reluctance Machine," *IEEE Trans. Power Electron.*, vol. 37, no. 11, pp. 13566-13576, Nov. 2022.

[24] E. Ofori, T. Husain, Y. Sozer and I. Husain, "A Pulse-Injection-Based Sensorless Position Estimation Method for a Switched Reluctance Machine Over a Wide Speed Range," *IEEE Trans. Ind. Appl.*, vol. 51, no. 5, pp. 3867-3876, Sept.-Oct. 2015.

[25] W. Wang, X. Zhao and S. Niu, "Predictive-Pulse-Injection-Based Dual-Inverter Complementary Sensorless Drive for 12/10 DC Vernier Reluctance Machine," *IEEE Trans. Power Electron.*, vol. 37, no. 7, pp. 8369-8378, July 2022.

[26] A. Khalil and I. Husain, "Four quadrant sensorless operation of a switched reluctance machine using fourier model," in *Proc. IEEE Annu. Power Electron. Spec. Conf.*, 2006.

[27] D. Zhou and H. Chen, "Four-Quadrant Position Sensorless Operation of Switched Reluctance Machine for Electric Vehicles over a Wide Speed Range," *IEEE Trans. Transp. Electrif.*, vol. 7782, no. c, pp. 1–13, 2021.

[28] T. Bamba, A. Komatsuzaki, and I. Miki, "Estimation of rotor position for switched reluctance motor at standstill," in *Proc. Fourth Power Convers. Conf. PCC-NAGOYA 2007 - Conf. Proc.*, pp. 259–263, 2007.

[29] J. Cai and Z. Deng, "Initial Rotor Position Estimation and Sensorless Control of SRM Based on Coordinate Transformation," *IEEE Trans. Instrum. Meas.*, vol. 64, no. 4, pp. 1004–1018, 2015.

[30] C. Gan, F. Meng, Z. Yu, R. Qu, Z. Liu and J. Si, "Online Calibration of Sensorless Position Estimation for Switched Reluctance Motors With Parametric Uncertainties," *IEEE Trans. Power Electron.*, vol. 35, no. 11, pp. 12307-12320, Nov. 2020.

[31] I. Husain and M. Ehsani, "Rotor position sensing in switched reluctance motor drives by measuring mutually induced voltages," *IEEE Trans. Ind. Appl.*, vol. 30, no. 3, pp. 665-672, May-June 1994.

[32] X. Zhou, B. Zhou, J. Yu, L. Yang and Y. Yang, "Research on Initial Rotor Position Estimation and Anti-Reverse Startup Methods for DSEM," *IEEE Trans. Ind. Electron.*, vol. 64, no. 4, pp. 3297-3307, April 2017.

[33] W. Wang, S. Niu and X. Zhao, "Integrating Sensing Coil Function into Field Winding for Initial Position Estimation of Nonsalient DC Vernier Reluctance Machine," *IEEE Trans. Power Electron.*, vol. 38, no. 3, pp. 2805-2810, March 2023.

[34] M. -W. Kim, J. Lee, M. Biswas and J. -W. Park, "New Acoustic Noise Reduction Method for Signal-Injection-Based IPMSM Sensorless Drive," *IEEE Trans. Power Electron.*, vol. 38, no. 3, pp. 3180-3190, March 2023.

WEIYU WANG is currently working toward the Ph.D. degree in electrical engineering with the Department of Electrical Engineering, Hong Kong Polytechnic University, Hong Kong, China.

His research interests include electrical machine drive and position-sensorless drive.

SHUANGXIA NIU (Sennior Member, IEEE) received the B.Sc. and M.Sc. degrees in electrical engineering from the School of Electrical Engineering and Automation, Tianjin University, Tianjin, China, in 2002 and 2005, respectively, and the Ph.D. degree in electrical engineering from the Department of Electrical and Electronic Engineering, The University of Hong Kong, Hong Kong, in 2009, all in electrical engineering.

Since 2009, she has been with The Hong Kong Polytechnic University, Hong Kong, where she is currently an Associate Professor with the Department of Electrical Engineering. She has authored or

coauthored over 100 articles in leading journals. Her research interests include novel electrical machines and drives, renewable energy conversion systems, and applied electromagnetics.

XING ZHAO (Member, IEEE) received the B.Eng. degree from Nanjing University of Aeronautics and Astronautics, Nanjing, China, in 2014, and the Ph.D. degree from The Hong Kong Polytechnic University, Hong Kong, China, in 2020, both in Electrical Engineering.

From Jul. 2019 to Jan. 2020, he was a Visiting Research Scholar with the Center for Advanced Power Systems, Florida State University, Tallahassee, USA. Between Jul. 2020 and Oct. 2021, he served as a Research Assistant Professor with the Department of Electrical Engineering, The Hong Kong Polytechnic University. Since Nov. 2021, he has been a Lecturer in the Department of Electronic Engineering with University of York, UK. He has authored or coauthored more than 50 technical papers in the international journals and conferences and holds six granted patents. His research interests include advanced electrical machines, motor drives, and power electronics for electric vehicles and renewable energy systems.